Analysis and Performance Enhancement of Wireless Power Transfer Systems With Intended Metallic Objects

Hui Wen Rebecca Liang, *Student Member, IEEE*, Hanwei Wang, Chi-Kwan Lee, *Senior Member, IEEE*, and S. Y. Ron Hui, *Fellow, IEEE*

***Abstract*—While detection of foreign or unintended metallic objects is an important topic for wireless power transfer (WPT), operation of WPT systems with intended metallic objects is largely an unchartered territory. This article presents a methodology for analyzing the effects of intended metallic object on a WPT system through the study of the magnetic field distribution and the use of a reduced-order equivalent model of the systems for comparing the WPT system with and without the metallic object. The methodology is applied to a metallic corona ring of low resistance used with a WPT system. The analysis quantifies how an intended metallic object could change the magnetic coupling between the transmitter and receiver coils, and alter the equivalent resonant tank parameters of the WPT system. Recompensation of the resonant tank can only enhance the power transfer capability but not the energy efficiency. The theory and practical verification of a new performance-enhancement method based on a combination of recompensating the resonant tanks and maximizing the equivalent mutual inductance of the Tx and Rx coils is presented. Such methodology provides a general approach to analyze WPT systems with or without relay resonators in the presence of intended metallic objects.**

***Index Terms*—Metallic objects, wireless power transfer (WPT).**

I. Introduction

WIRELESS power transfer (WPT) has already reached the commercialization stage in some applications, such as industrial manufacturing facilities [1] and smart-phones [2], and is currently being extended to medical implants [3] and electric vehicles [4]. Recent research into various new WPT structures, such as wireless bearings [5] and ball-joints [6] structures, also offer new opportunities to widen the WPT application scope. Foreign metallic object detection (FoD) has been raised in WPT industry as an important topic, particularly for wireless charging pads for consumer electronics and electric vehicles. FoD techniques proposed by the industry are primarily based on the detection of the change of mutual coupling or power difference between input and output [7]–[11]. The purpose of such detection is to stop the wireless charging once foreign objects are detected. However, operation of WPT systems with intended metallic objects is largely not addressed in the existing literature.

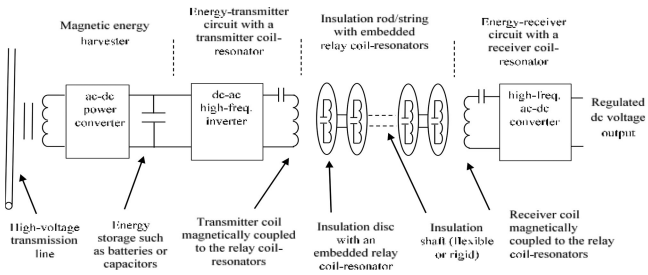

Fig. 1. Schematic of the wireless power transfer system for power systems [13].

This article addresses a new research discipline of studying the effects of intended metallic object in WPT systems. With the fast emerging smart grid technology demanding more distributed sensors to monitoring the power systems, one recent innovation is the utilization of the domino WPT systems [12] in the form of a high-voltage (HV) insulation rod (see Fig. 1) for powering online monitoring systems mounted on the top of the HV transmission towers [13]. With the use of a current transformer to harvest energy from the magnetic field around the transmission cable, HV insulation rods with coil-resonators embedded inside the insulation discs (see Fig. 2) for WPT applications have been proposed as a "weather-independent" stable power supply for the monitoring system mounted on the HV transmission tower (see Fig. 3). For a transmission voltage above 230 kV, metallic corona ring is usually used with the insulation rod to avoid corona discharge. This corona ring is typically made of aluminum and is a form of intended metallic object used with the HV insulation rod with WPT capability. This article presents a new methodology of

Manuscript received April 16, 2020; revised June 10, 2020; accepted July 13, 2020. Date of publication July 24, 2020; date of current version September 22, 2020. This work was supported by Hong Kong Research Grant Council through the General Research Fund under Grant 17203517. The work of Hui Wen Rebecca Liang was supported by the Hong Kong Postgraduate Fellowship. Recommended for publication by Associate Editor M. Ponce-Silva. *(Corresponding author: S. Y. Ron Hui.)*

Hui Wen Rebecca Liang and Chi-Kwan Lee are with the Department of Electrical and Electronic Engineering, The University of Hong Kong, Hong Kong (e-mail: rebeccaliang0425@gmail.com; cklee@eee.hku.hk).

Hanwei Wang is with the Department of Electrical and Computer Engineering, University of Illinois at Urbana-Champaign, Urbana, IL 61801 USA (e-mail: hanweiw2@illinois.edu).

S. Y. Ron Hui is with the Department of Electrical and Electronic Engineering, The University of Hong Kong, Hong Kong, and also with the Department of Electrical and Electronic Engineering, Imperial College London, SW7 2AZ London, U.K. (e-mail: ronhui@eee.hku.hk).

Color versions of one or more of the figures in this article are available online at https://ieeexplore.ieee.org.

Digital Object Identifier 10.1109/TPEL.2020.3011761

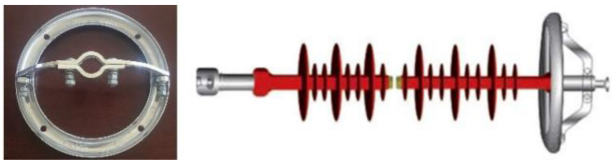

Fig. 2. Corona ring JYH-250 and its position in an insulation string.

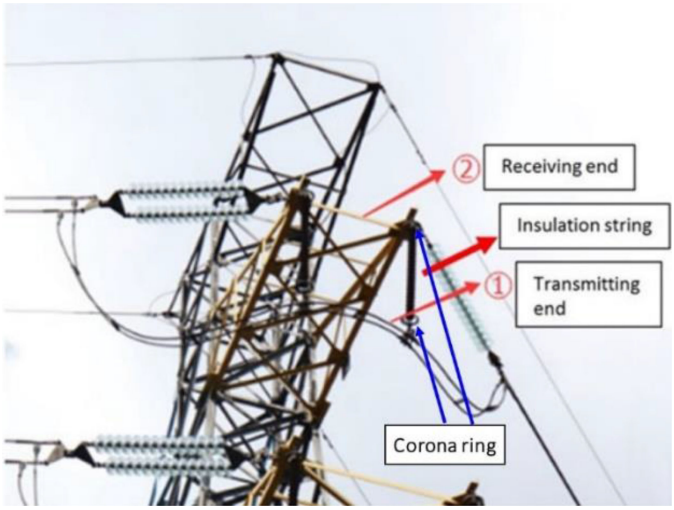

Fig. 3. Use of insulation rods for WPT transfer to power online monitoring systems on top of the HV transmission tower.

analyzing the effects of the metallic objects through the study of the magnetic distribution and the use of a reduced-order model. The study focuses both on the power transfer capability and system energy efficiency. The methodology can be applied to WPT systems with or without relay resonators.

II. Analysis of WPT System With Intended Metallic Object

Fig. 3 illustrates the application concept, in which energy is harvested from the transmitting end ①, then wirelessly transferred through the relay resonator embedded in the insulation string to the receiving end ②. The corona ring JYH-250 used in this study is made up of material Al-1050 with over 99% aluminium and a relative magnetic permeability of 1.000022. It can therefore be modeled as an inductor with inductance L_C in series with resistance R_C. In the initial study, we focus on the transmitter coil and a receiver coil with the corona ring placed in the middle (see Fig. 4). The analysis will be extended to a multiple-coil system with relay resonators (included in Appendix).

A finite-element simulation of the magnetic field distribution in a two-coil WPT system with and without the corona ring is first conducted to highlight the problems introduced by the metallic object. Fig. 5(a) and (b) shows the finite-element simulation results using ANSYS Maxwell for a two-coil WPT system *with* and *without* an aluminum corona ring. Tx and Rx stand for the transmitter and receiver coils while C stands for the corona ring. It can be observed that the magnetic field distribution is

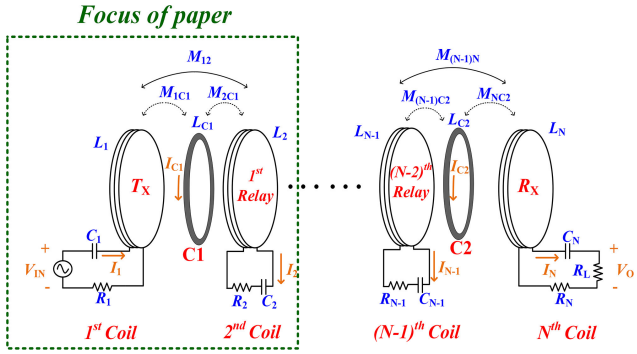

Fig. 4. WPT system with N-relay coils and two corona rings C_1 and C_2.

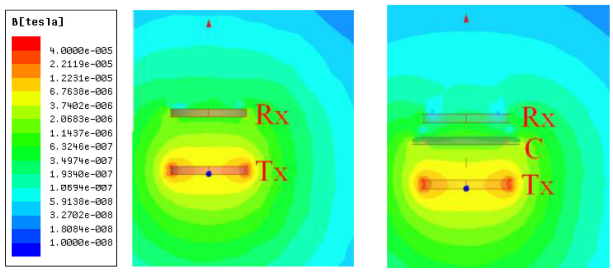

Fig. 5. Finite-element simulation of a two coil system (a) without ring (TR system) and (b) with ring (TCR system).

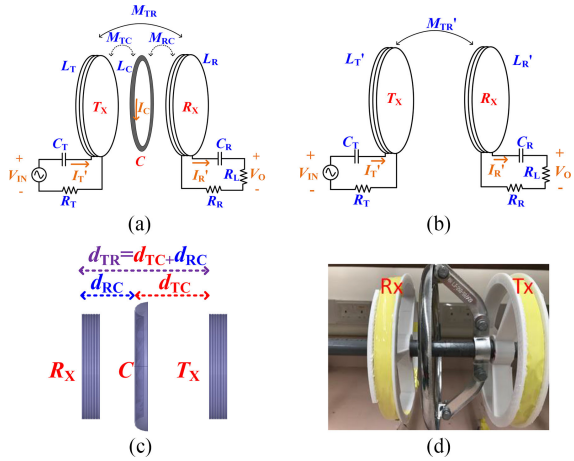

Fig. 6. TCR system. (a) Original system. (b) Equivalent reduced-order model. (c) Positioning and distance of coils and ring. (d) Hardware setup.

obviously affected by the metallic ring. By comparing the two diagrams, it can be observed that the magnetic field induced around the Rx coil is weaker with the metallic ring than without the metallic ring. It is therefore necessary to quantify this effect.

A. System Description

To understand how corona rings affect system performance when it is included in a domino WPT system, we must first understand how it affects a two-coil system. Considering a 2-coil transmitter–receiver (TR) system such as the one shown in Fig. 6(a) by ignoring the ring C in between transmitter Tx

and receiver Rx, the impedance matrix can be expressed as (1), where $Z_T = j(\omega L_T - \frac{1}{\omega C_T}) + R_T$ and $Z_R = j(\omega L_R - \frac{1}{\omega C_R}) + R_R$. L_T and L_R refer to the transmitter and receiver coil inductance, respectively. C_T and C_R are their corresponding compensation capacitance according to $(\omega L_T - \frac{1}{\omega C_T}) = (\omega L_R - \frac{1}{\omega C_R})$ for maximum power transfer capability [14]. R_T and R_R are the respective parasitic resistances, R_L the load resistance, and M_{TR} is the mutual inductance between the two coils. $\omega = 2\pi f$, where f stands for the operating frequency

$$\mathbf{Z_{TR}} = \begin{bmatrix} Z_T & j\omega M_{TR} \\ j\omega M_{TR} & Z_R + R_L \end{bmatrix}. \tag{1}$$

This 2×2 matrix is useful in determining the characteristics of a two-coil WPT system. For any given input voltage V_{IN}, the phasor currents $\mathbf{I_T}$ and $\mathbf{I_R}$ in Tx and Rx could be found by performing simple matrix calculation

$$\begin{bmatrix} V_{\mathrm{IN}} \\ 0 \end{bmatrix} = \mathbf{Z_{TR}} \times \begin{bmatrix} \mathbf{I_T} \\ \mathbf{I_R} \end{bmatrix}. \tag{2}$$

The system energy efficiency of a TR system can be expressed as

$$\eta_{TR} = \frac{P_O}{P_O + P_T + P_R} = \frac{{I_R}^2 R_L}{{I_T}^2 R_T + {I_R}^2 (R_R + R_L)} = \frac{R_L}{(\frac{I_T}{I_R})^2 R_T + R_R + R_L}. \tag{3}$$

$P_O = {I_R}^2 R_L$ is the output power, $P_T = {I_T}^2 R_T$ and $P_R = {I_R}^2 R_R$ are the power loss caused by the coil resistors R_T and R_R. It can be seen from (3) that the ratio of rms currents I_T/I_R is very important in the efficiency of system.

In the case where a corona ring is added in between $\mathrm{T_X}$ and $\mathrm{R_X}$ like in Fig. 6(a), the impedance matrix turns into a 3×3 matrix as in (4), where Z_T and Z_R are as mentioned before and $Z_C = j\omega L_C + R_C$. L_C and R_C stand for the corona ring inductance and series resistance while M_{TC} and M_{RC} are the mutual inductance between the ring and L_T or L_R. The system characteristics are described by (5). $\mathbf{I_T}'$ and $\mathbf{I_R}'$ both have apostrophes to distinguish them from $\mathbf{I_T}$ and $\mathbf{I_R}$ in the matrix shown in (2) since different results are expected due to the interference of corona ring

$$\mathbf{Z_{TCR}} = \begin{bmatrix} Z_T & j\omega M_{TC} & j\omega M_{TR} \\ j\omega M_{TC} & Z_C & j\omega M_{RC} \\ j\omega M_{TR} & j\omega M_{RC} & Z_R + R_L \end{bmatrix} \tag{4}$$

$$\begin{bmatrix} V_{\mathrm{IN}} \\ 0 \\ 0 \end{bmatrix} = \mathbf{Z_{TCR}} \times \begin{bmatrix} \mathbf{I_T}' \\ \mathbf{I_C} \\ \mathbf{I_R}' \end{bmatrix}. \tag{5}$$

Efficiency for this transmitter-corona ring-receiver (TCR) system can be written as

$$\eta_{TCR} = \frac{P_O}{P_O + P_T + P_R + P_C} = \frac{{I_R}'^2 R_L}{{I_T}'^2 R_T + {I_R}'^2 (R_R + R_L) + {I_C}^2 R_C} = \frac{R_L}{(\frac{I_T'}{I_R'})^2 R_T + R_R + R_L + (\frac{I_C}{I_R'})^2 R_C} \tag{6}$$

where $P_O = {I_R}'^2 R_L$is the output power, $P_T = {I_T}'^2 R_T$, $P_R = {I_R}'^2 R_R$, and $P_C = {I_C}^2 R_C$ are the power loss caused by the coil resistors R_T and R_R, and the ring resistance R_C.

TABLE I
SYSTEM PARAMETERS FOR A 2-COIL SYSTEM WITH/WITHOUT CORONA RING

Coil and ring specifications					
Transmitter (Tx)		Corona Ring		Receiver (Rx)	
L_{T}	48.6 μH	L_{C}	341 nH	L_{R}	48.6 μH
C_{T}	52.2 nF			C_{R}	52.2 nF
R_{T}	170 mΩ	R_{C}	2 mΩ	R_{R}	170 mΩ
Before ring insertion (without corona ring)					
Distances between coils (mm)					
d_{TR} 150					
Mutual inductance M_{kj} (μH)					
M_{TR} 3.09					
After ring insertion (with corona ring)					
Distances between coils and ring (mm)					
d_{TC} 100			d_{RC} 50		
Mutual inductance M_{kj} (μH)					
M_{TR} 3.09					
M_{TC} 0.59			M_{RC} 1.38		

The system parameters are listed in Table I with and without the metallic ring. Both Tx and Rx coils are identical and compensated at 100 kHz ($C_T = C_R = 52.2$ nF). The corona ring is modeled using the parameters obtained by ANSYS Maxwell, $L_C = 341$ nH and $R_C \approx 2$ mΩ. In the case without ring, distance d_{TR} between the two coils Tx and Rx is 150 mm, which is equal to $d_{TC} + d_{RC}$. Distances d_{TR}, d_{TC}, and d_{RC} are depicted in Fig. 6(c).

B. System Analysis via the Reduced-Order Equivalent Model

A reduced-order model is introduced here to aid in the comparison of the two systems with and without the metallic ring. First, the input impedance of the TR system can be found by dividing the input voltage by input current $Z_{\mathrm{inTR}} = V_{\mathrm{IN}}/\mathbf{I_T}$, which results in

$$Z_{\mathrm{inTR}} = Z_T + \frac{\omega^2 {M_{TR}}^2}{Z_R + R_L}. \tag{7}$$

Solving for $V_{\mathrm{IN}}/\mathbf{I_T}'$ from (5), the new input impedance for a TCR system Z_{inTCR} could be arranged in a similar fashion

$$Z_{\mathrm{inTCR}} = Z_T + \frac{\omega^2 {M_{TC}}^2}{Z_C} + \frac{\omega^2 (M_{TR} - j\omega \frac{M_{TC} M_{RC}}{Z_C})^2}{Z_R + \frac{\omega^2 {M_{RC}}^2}{Z_C} + R_L}. \tag{8}$$

Observing the above equation, the matrix in (4) can easily be rearranged as the reduced-order model

$$\mathbf{Z_{TCR\_eq}} = \begin{bmatrix} Z_T - \frac{(j\omega M_{TC})^2}{Z_C} & j\omega M_{TR} - \frac{j\omega M_{TC}\cdot j\omega M_{RC}}{Z_C} \\ j\omega M_{TR} - \frac{j\omega M_{TC}\cdot j\omega M_{RC}}{Z_C} & Z_R - \frac{(j\omega M_{RC})^2}{Z_C} + R_L \end{bmatrix}. \tag{9}$$

It can be seen that the effect of the ring can be mapped onto Z_T, Z_R, and mutual inductance M_{TR}. Substituting $Z_T = j(\omega L_T - \frac{1}{\omega C_T}) + R_T$, $Z_R = j(\omega L_R - \frac{1}{\omega C_R}) + R_R$, and $Z_C = j\omega L_C$ into the above matrix gives the following result:

$$\mathbf{Z_{TCR\_eq}} = \begin{bmatrix} j(\omega L_T{}' - \frac{1}{\omega C_T}) + R_T{}' & j\omega M_{TR}{}' + R_{TR}{}' \\ j\omega M_{TR}{}' + R_{TR}{}' & j(\omega L_R{}' - \frac{1}{\omega C_R}) + R_R{}' + R_L \end{bmatrix}. \tag{10}$$

where $L_T{}'$, $L_R{}'$, $R_T{}'$, and $R_R{}'$ denote, respectively the equivalent Tx and Rx coil inductances and parasitic resistances after a corona ring is placed in the system. While $M_{TR}{}'$ stands for their equivalent mutual inductance, $R_{TR}{}'$ is an introduced parameter to indicate that the equivalent induced voltage on Tx (Rx) contains a part that is in phase with the Rx (Tx) current. These parameters are derived as

$$L_T{}' = L_T - \frac{M_{TC}{}^2}{L_C} \cdot \frac{1}{1 + 1/Q_C{}^2} \approx L_T - \frac{M_{TC}{}^2}{L_C} \tag{11}$$

$$L_R{}' = L_R - \frac{M_{RC}{}^2}{L_C} \cdot \frac{1}{1 + 1/Q_C{}^2} \approx L_R - \frac{M_{RC}{}^2}{L_C} \tag{12}$$

$$M_{TR}{}' = M_{TR} - \frac{M_{TC}M_{RC}}{L_C} \cdot \frac{1}{1 + 1/Q_C{}^2} \approx M_{TR} - \frac{M_{TC}M_{RC}}{L_C} \tag{13}$$

$$R_T{}' = R_T + \frac{M_{TC}{}^2 R_C}{L_C{}^2} \cdot \frac{1}{1 + 1/Q_C{}^2} \approx R_T + \frac{M_{TC}{}^2 R_C}{L_C{}^2} \tag{14}$$

$$R_R{}' = R_R + \frac{M_{RC}{}^2 R_C}{L_C{}^2} \cdot \frac{1}{1 + 1/Q_C{}^2} \approx R_R + \frac{M_{RC}{}^2 R_C}{L_C{}^2} \tag{15}$$

$$R_{TR}{}' = \frac{M_{TC}M_{RC}R_C}{L_C{}^2} \cdot \frac{1}{1 + 1/Q_C{}^2} \approx \frac{M_{TC}M_{RC}R_C}{L_C{}^2} \tag{16}$$

where $Q_C = \omega L_C/R_C$. Note that $Q_C >> 1$ for the case with metal ring and thus, $\frac{1}{1+1/Q_C{}^2} \approx 1$. The corresponding current and voltage matrix can be modified as

$$\begin{bmatrix} V_{\mathrm{IN}} \\ 0 \end{bmatrix} = \mathbf{Z_{TCR\_eq}} \times \begin{bmatrix} \mathbf{I_T}{}' \\ \mathbf{I_R}{}' \end{bmatrix}. \tag{17}$$

This reduced-order (2×2) equivalent model is mathematically identical to that represented by the original 3×3 matrix in (4) and (5). Direct comparison of the system matrix elements in (1) without the metallic ring, and those in (10)–(16) with the metallic ring can therefore provide important information to quantify the effects of the metallic ring on the WPT system.

TABLE II
REDUCED-ORDER EQUIVALENT MODEL PARAMETERS FOR A 2-COIL, 1-RING SYSTEM

Self-inductance L_{kk} (μH)			
L_T' (T_x)	47.58 μH	L_R' (R_x)	43.02 μH
C_T (brc*): C_T' (arc**):	52.2 nF 47.2 nF	C_R	52.2 nF
R_T'	176 mΩ	R_R'	202.8 mΩ
Distances between coils and ring (mm)			
d_{TR} 150			
Mutual inductance M_{TR}' and factor R_{TR}'			
M_{TR}' 0.712 μH R_{TR}' 14 mΩ			

*b.rc: before recompensation.
**a.rc: after recompensation.

Several important concluding remarks can be made as follows.

1) Equations (11) and (12) indicate that the equivalent self-inductance of the transmitter coil and receiver coil are reduced by factors depending on their respective mutual coupling coefficients with the corona ring (M_{TC} and M_{RC}) and the self-inductance of the corona ring (L_C).
2) The mutual inductance between the transmitter and receiver coil in (13) is reduced by a term depending on L_C and the product of M_{TC} and M_{RC}.
3) As energy efficiency is proportional to the product of the mutual coupling coefficient and the quality factors of the windings, (13) quantifies how the presence of the metallic object could affect the distribution of the magnetic field and provides the measure of the reduction of the mutual coupling coefficient.
4) Minimizing the negative term in (13) can mitigate the negative effects of the intended metallic object on energy efficiency.
5) Equations (14) and (15) show that the equivalent resistances of the transmitter and receiver coils are increased by factors depending on the coupling coefficients with the corona ring (M_{TC} and M_{RC}), the self-inductance of the corona ring (L_C), and the series resistance of the ring (R_C).
6) The increase in equivalent R_T and R_R results in additional power loss.
7) The equivalent induced voltage on transmitter (receiver) coil has an additional component that is in phase with the receiver (transmitter) current and scaled by the factor in (16).

The equivalent parameters calculated according to (11)–(16) for the circuit parameters in Table I are presented in Table II. Note that L_R is reduced more significantly when compared to L_T due to the smaller distance (and thus, higher mutual inductance M_{RC}) in between the receiver and the ring. The increase in R_T is much smaller when compared to R_R for the same reason. Mutual inductance drops to $M_{TR}{}' = 0.712\ \mu$H, which is only 23% of

its original $M_{TR} = 3.09\ \mu$H in the TR system. Moreover, since $|\omega M_{TR}{}'| >> R_{TR}{}'$, the effect of $R_{TR}{}'$ is neglected in all the following analyses.

Next, to find the optimal operating frequency for maximum efficiency in a TR system, one can search the condition to maximize the current gain I_R/I_T in (3)

$$\frac{I_R}{I_T} = \frac{\omega^2 C_R M_{TR}}{\sqrt{\left(\omega^2 C_R L_R - 1\right)^2 + \left[\omega C_R (R_R + R_L)\right]^2}}. \tag{18}$$

The condition for maximizing I_R/I_T in (3) can be obtained by differentiating (18) with respect to ω and then, equating it to zero so as to determine the optimal operating frequency as

$$f_{\text{opt\_TR}} = \frac{\omega_{\text{opt\_TR}}}{2\pi} = \frac{1}{2\pi\sqrt{L_R C_R - {C_R}^2 (R_L + R_R)^2/2}}. \tag{19}$$

For TCR systems, equations like the above can be written in the same fashion but replacing L_R with $L_R{}'$, R_R with $R_R{}'$, and M_{TR} with $M_{TR}{}'$. Note that the efficiency in (6) can first be rearranged as the following with $R_{TR}{}'$ neglected:

$$\eta_{\text{TCR\_eq}} \approx \frac{P_O}{P_O + P_T{}' + P_R{}'} = \frac{{I_R{}'}^2 R_L}{{I_T{}'}^2 R_T{}' + {I_R{}'}^2 (R_R{}' + R_L)} = \frac{R_L}{\left(\frac{I_T{}'}{I_R{}'}\right)^2 R_T{}' + R_R{}' + R_L}. \tag{20}$$

The I'_R/I'_T ratio above can be obtained as (21) and the new optimal operating frequency as (22) in the following:

$$\frac{I_R{}'}{I_T{}'} \approx \frac{\omega^2 C_R M_{TR}{}'}{\sqrt{\left(\omega^2 C_R L_R{}' - 1\right)^2 + \left[\omega C_R (R_R{}' + R_L)\right]^2}} \tag{21}$$

$$f_{\text{opt\_TCR}} \approx \frac{1}{2\pi\sqrt{L_R{}' C_R - {C_R}^2 (R_L + R_R{}')^2/2}}. \tag{22}$$

Note that the operating frequency for the maximum efficiency is merely dependent on the secondary-side compensation and independent of primary-side compensation, regardless of whether the system is interfered by the metal ring or not.

Comparing (18)–(22) leads to the following important remarks.

1) Equation (20) indicates that it is necessary to minimize the ratio of I'_T/I'_R or to maximize I'_R/I'_T in (21) in order to maximize the energy efficiency in a WPT system with intended metallic object.
2) Minimizing $R_T{}'$ and $R_R{}'$ can increase the energy efficiency in a WPT system with intended metallic object according to (20).
3) The metallic object will cause the maximum efficiency to occur at a higher operating frequency (i.e., $f_{\text{opt\_TCR}} > f_{\text{opt\_TR}}$) due to the smaller equivalent self-inductance of the receiver coil as reflected from a comparison of (19) and (22).
4) The change of the optimal operating frequency by the metallic object will affect the power transfer capability unless the system is recompensated.
5) Equation (21) shows that to maximize I'_R/I'_T for maximum energy efficiency is to maximize M'_{TR} if the receiver parameters do not change.

III. Performance Enhancement for System With Intended Metallic Object

This section presents a new twofold performance-enhancement methodology based on the combination of recompensating the resonant circuit and redesigning the transmitter coil for WPT system with intended metallic object.

A. Recompensation of C_T: Reshaping Power Capability

The reduced-order model based on (10)–(16) reflects the effects of metallic ring on the modified self- and mutual inductances of the coils. This problem is simplified to the compensation of a simple 2-coil system. The TCR system needs to be recompensated with new transmitter-side capacitor $C_T{}'$ so that $(\omega_{\text{opt\_TCR}} L_T{}' - \frac{1}{\omega_{\text{opt\_TCR}} C_T{}'}) = (\omega_{\text{opt\_TCR}} L_R{}' - \frac{1}{\omega_{\text{opt\_TCR}} C_R})$. The recompensation capacitance, denoted as $C_T{}'$, is derived as

$$C_T{}' = \frac{C_R}{C_R (L_T{}' - L_R{}') \omega_{\text{opt\_TCR}}{}^2 + 1}. \tag{23}$$

The recompensation of the resonant circuit reduces the impedance of the power flow path, and therefore, will enhance the power flow capacity at the new operating (maximum efficiency) frequency $f_{\text{opt\_TCR}}$. The capacitor re-compensated according to (23) for the system in Tables I and II is listed in Table II.

B. Redesigning Transmitter Size to Maintain High $M_{TR}{}'$ Value

Recompensation of C_T illustrated previously only improves the power transfer capability. But the energy efficiency can be further and significantly improved by redesigning the transmitter coil by minimizing the reduction of M'_{TR} in (13). The reduction of energy efficiency caused by the metallic ring depends highly on the parameter $M_{TR}{}'$. Notice that although the increase in R_T and R_R puts on additional power loss, the effect of both these parameters on efficiency are outweighed by the decreased $I_R{}'/I_T{}'$ ratio in the case with metal ring. The study in this article, therefore, focuses on the improvement of $M_{TR}{}'$.

Since all receiver-side parameters $\{L_R{}', C_R, R_R, M_{RC}, d_{RC}\}$ are kept fixed, the optimal frequency $f_{\text{opt·TCR}}$ in (22) will not change if $M_{TR}{}'$ is changed. Equation (21) further states that the ratio of rms currents $I_R{}'/I_T{}'$ is proportional to $M_{TR}{}'$

$$\frac{I_R{}'}{I_T{}'} \propto M_{TR}{}' \tag{24}$$

since $\{f_{\text{opt\_TCR}}, L_R{}', C_R, R_R{}', R_L\}$ are fixed variables. Next, substituting (21) into (20), the energy efficiency is merely dependent on ${M_{TR}{}'}^2/R_T{}'$, in which, the effect of $M_{TR}{}'$ is significant due to its square function. Maximizing $M_{TR}{}'$ will increase the energy efficiency.

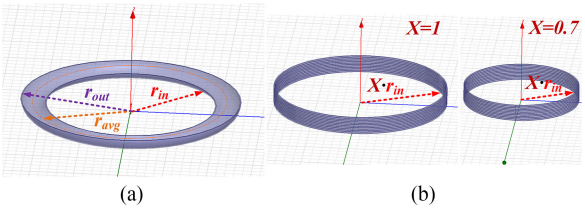

Fig. 7. Indication of ring and transmitter radius. (a) Ring outer radius r_{out}, inner radius r_{in}, and average radius r_{avg}. (b) Transmitter with same radius as r_{in}. (c) Transmitter with radius 0.7 times that of r_{in}.

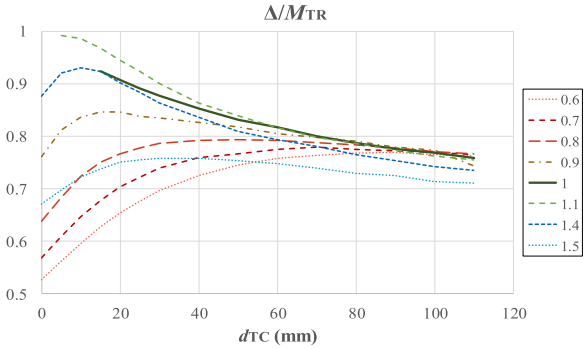

Fig. 8. Variations of the mutual inductance reduction term with d_{TC} for a range of dimension ratio X.

Rearranging (13) as

$$M_{TR}{}' = M_{TR}\left(1 - \frac{\Delta}{M_{TR}}\right) \tag{25}$$

where $\Delta = M_{TC}M_{RC}/L_C$. From (25), there are two ways to increase $M_{TR}{}'$.

1) Increase M_{TR}.
2) Lower the ratio Δ/M_{TR}, which is an indication of the amount of drop on M_{TR} due to ring insertion. A small ratio implies that the equivalent mutual coupling is less affected by the ring.

In the study mentioned in this article, we discover that energy efficiency in a WPT system with intended metallic object can be enhanced through increasing M'_{TR} by:

1) reducing the transmission distance d_{TR} in order to increase M_{TR};
2) redesigning the dimension ratio of the transmitter coil and metallic ring away from unity in order to reduce M_{TC} in Δ.

On the surface, shortening the distance d_{TR} between the Tx coil and Rx coil will reduce d_{TC} which may increase M_{TC} and become detrimental to the energy efficiency. However, this issue can be avoided by redesigning the transmitter coil with a dimension different from that of the metallic ring. Let the ratio of the diameters of the transmitter coil and the corona ring be X. An example of a coil with a ratio $X = 0.7$ is shown in Fig. 7.

Fig. 8 shows the theoretical results of how the ratio Δ/M_{TR} changes with the distance d_{TC} from 0–110 mm while d_{RC} is kept constant at 50 mm for a TCR system for a range of X from 0.6 to 1.5. All other system parameters are the same as the examples in Table II. $X = 0.7$ means that the transmitter coil

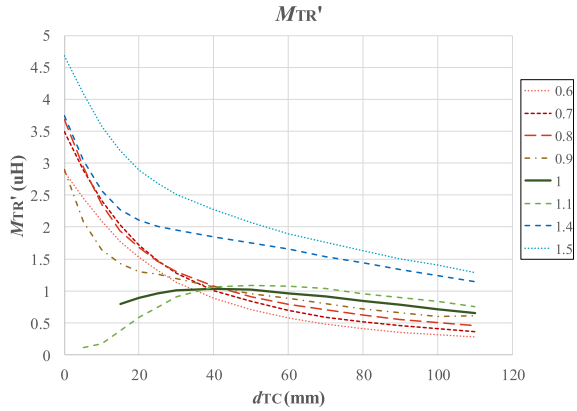

Fig. 9. Variations of the equivalent mutual inductance with d_{TC} for a range of dimension ratio X.

diameter is 0.7 times the ring inner diameter (r_{in}). The example used in the previous sections are when $X \approx 1$; its curve is in solid dark green in the charts. For the ring used in the article, Fig. 2(a), $r_{\text{in}} = 10.25$ cm, the ring's outer radius $r_{\text{out}} \approx 1.2 r_{\text{in}}$ and average radius $r_{\text{avg}} = (r_{\text{out}} + r_{\text{in}})/2 \approx 1.1 r_{\text{in}}$. From Fig. 8, it can be observed that as X departs from unity and d_{TC} decreases, the negative reduction term of the equivalent mutual inductance in (13) decreases too. For example, when $X = 0.7$, the mutual inductance reduction term is reduced to 0.7 for a d_{TC} of 20 mm. Fig. 9 shows the corresponding equivalent mutual inductance of the WPT system with the metallic ring. Comparing the cases of $X = 0.7$ and $X = 1.0$ at $d_{TC} = 20$ mm, M'_{TR} can be increased from 0.85 to 1.7 μH.

IV. Experimental Results

The scientific principles to enhance the performance of a WPT system with intended metallic object can be summarized as: 1) recompensating the resonant tank based on the reduced-order model and 2) redesigning the transmission coil to maximize the equivalent mutual inductance M'_{TR} as explained in the previous section. This section provides the experimental proof of these principles. A hardware prototype is set up to evaluate the theoretical predictions and practical measurements.

A. WPT TCR System

Fig. 6 shows the first hardware setup for a TCR system. Tx and Rx coils are single-layered 11-turn winding with coil radius = 10 cm. The corona ring in the setup is the JYH-250 shown in Fig. 2 with r_{in} of 10.25 cm and outer radius r_{out} of approximately 12.3 cm. Fig. 10 shows the energy efficiency and power transfer capability of the original 2-coil system measured under $V_{\text{IN,pk-pk}} = 5$ V without the metallic ring with the following parameters: $d_{TR} = 150$ mm. Maximum energy efficiency of about 80% occurs at about 100 kHz at which over 4 W of power can be transferred.

Then, a corona ring is inserted between the Tx and Rx coils with $d_{TC} = 100$ mm and $d_{RC} = 50$ mm. Fig. 11(a) shows the corresponding energy efficiency and power transfer capability. It is noted that the maximum energy efficiency has shifted from

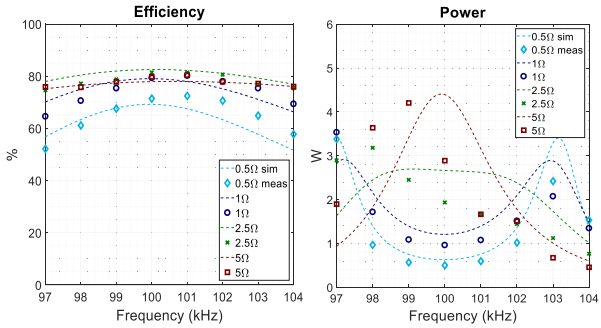

Fig. 10. Theoretical and measured efficiency and power plots of a two-coil system without corona ring (TR system). Circuit parameters: $L_T = L_R = 48.6\ \mu$H, $M_{TR} = 3.09\ \mu$H, $C_T = C_R = 52.2$ nF, $f_{\text{opt\_TR}} = 100$ kHz.

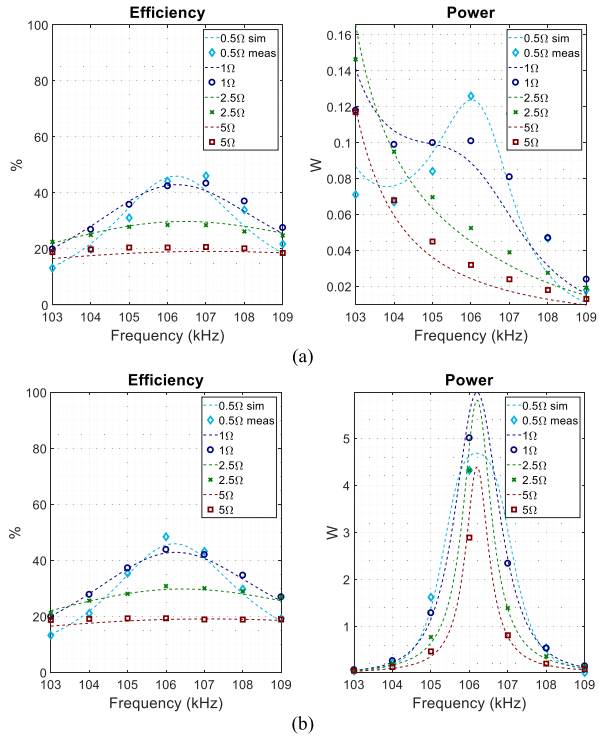

Fig. 11. Theoretical and measured efficiency and power plots of a two-coil system with corona ring (TCR system). Circuit parameters: $L_T = L_R = 48.6\ \mu$H ($L_T{}' = 47.58\ \mu$H, $L_R{}' = 43.02$), $L_C = 341$ nH, $M_{TR} = 3.09\ \mu$H ($M_{TR}{}' = 712$ nH), $M_{TC} = 0.59\ \mu$H, $M_{RC} = 1.38\ \mu$H, $C_R = 52.2$ nF, $R_T = 170\ \text{m}\Omega$, $R_R = 170\ \text{m}\Omega$ ($R_T{}' = 176\ \text{m}\Omega$, $R_R{}' = 202.8\ \text{m}\Omega$), $f_{\text{opt·TR}} = 106.3$ kHz and transmitter compensated capacitors are (a) not recompensated: $C_T = 52.2$ nF and (b) recompensated: $C_T{}' = 47.2$ nF.

100 kHz to about 106 kHz and is reduced from 80% to 45%. Also, the power transfer is reduced significantly from over 4 W to less than 0.1 W. The frequency shift of the maximum efficiency point is expected from (22).

After recompensating the resonant tank at the new optimal frequency of 106 kHz, Fig. 11(b) shows the modified energy efficiency and power transfer capability plots. It is interesting to note that the maximum energy efficiency remains at 45% as predicted, but the power transfer can be higher than 5 W. Figs. 12 and 13 shows the in/output current and voltage waveforms before and after recompensation at 100 and 106 kHz.

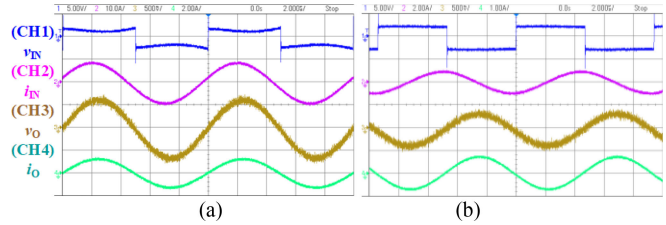

Fig. 12. Waveforms of a two-coil TCR system without recompensation and load resistance of 0.5 Ω. (a) 100 kHz [CH1: 5 V/div, CH2: 10 A/div, CH3: 500 mV/div, CH4: 2 A/div]. (b) 106 kHz [CH1: 5 V/div, CH2: 2 A/div, CH3: 500 mV/div, CH4: 1 A/div].

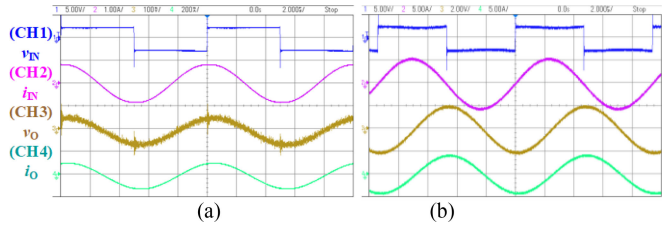

Fig. 13. Waveforms of a two-coil TCR system after recompensation and load resistance of 0.5 Ω. (a) $f = 100$ kHz [CH1: 5 V/div, CH2: 1 A/div, CH3: 100 mV/div, CH4: 200 mA/div]. (b) 106 kHz [CH1: 5 V/div, CH2: 5 A/div, CH3:2 V/div, CH4: 5 A/div].

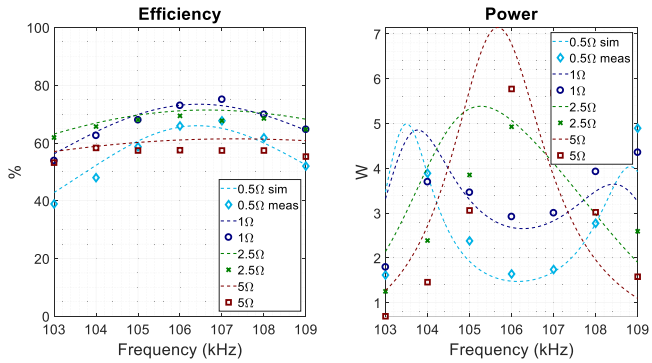

Fig. 14. Theoretical and measured efficiency and power plots of a two-coil system with corona ring (TCR system). Circuit parameters: $L_T = 30\ \mu$H, $L_R = 48.6\ \mu$H ($L_T{}' = 26.9\ \mu$H, $L_R{}' = 42.9$), $L_C = 341$ nH, $M_{TR} = 6.0\ \mu$H ($M_{TR}{}' = 1.8\ \mu$H), $M_{TC} = 1.0\ \mu$H, $M_{RC} = 1.4\ \mu$H, $C_T = 84.3$ nF, $C_R = 52.2$ nF, $R_T = 140\ \text{m}\Omega$, $R_R = 170\ \text{m}\Omega$ ($R_T{}' = 157\ \text{m}\Omega$, $R_R{}' = 202.8\ \text{m}\Omega$), $f_{\text{opt\_TCR}} = 106.4$ kHz.

To further increase the energy efficiency, we choose a new Tx coil with $X = 0.7$ for demonstration of the proposed principles. The test conditions are: $X = 0.7$, $d_{TC} = 20$ mm and $d_{CR} = 50$ mm. The energy efficiency and power transfer capability plots are shown in Fig. 14. The energy efficiency can now be raised to over 70% and the power transfer capability is about 6 W.

B. WPT System TCR System With a Relay Coil-Resonator

A set of experiments have also been conducted for a three-coil system *with* and *without* corona ring, positioned as shown in Fig. 15. The relay coil is designed with inductance $L_{RC} = 48.6\ \mu$H and compensated with $C_{RC} = 52.2$ nF at 100 kHz. Other circuit parameters are listed in the caption of Fig. 16.

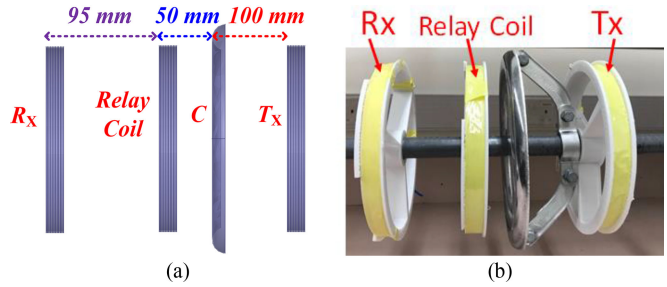

Fig. 15. (a) Arrangement of a TCR system with a relay coil-resonator and its (b) hardware setup.

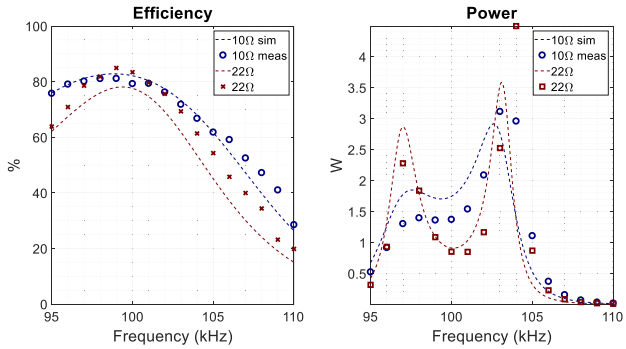

Fig. 16. Simulated and measured efficiency and power plots of a three coil system *without* corona ring. Circuit parameters: $L_T = L_{RC} = L_{RC} = 48.6$ μH, $M_{TR} = 1.09$ μH, $M_{RC\text{-}R} = 6.52$ μH, $M_{RC\text{-}T} = 3.09$ μH, $C_T = C_R = C_{RC} = 52.2$ nF.

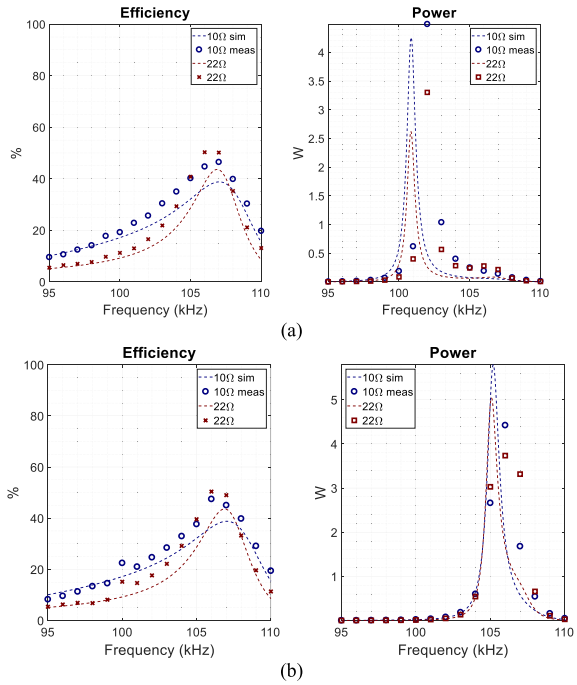

Fig. 17. Simulated and measured efficiency and power plots of a three coil system *with* corona ring between the Tx and the relay coil. Circuit parameters: $L_T = L_{RC} = L_R = 48.6$ μH ($L_T{}' = 47.7$ μH, $L_{RC}{}' = 42.4$, $L_R{}' = 48.2$), $L_C = 341$ nH, $M_{TR} = 1.09$ μH, $M_{TC} = 0.57$ μH, $M_{RC} = 0.36$ μH, $M_{RC\text{-}C}$ (mutual between relay and ring) $= 1.45$ μH, $M_{RC\text{-}R} = 6.52$ μH, $M_{RC\text{-}T} = 3.09$ μH, $C_R = C_{RC} = 52.2$ nF and transmitter capacitance (a) not recompensated $C_T = 52.2$ nF and (b) recompensated $C_T{}' = 48$ nF.

Fig. 16 shows the efficiency and power for the 3-coil system without the ring. Maximum efficiency occurs in the vicinity of 100 kHz, which is the resonant frequency of the three coils. With the insertion of the ring, the maximum efficiency frequency is shifted to approximately 106.9 kHz, as shown in Fig. 17(a). This frequency is the equivalent resonant frequency of the relay coil $1/(2\pi\sqrt{L_{RC}{}'C_{RC}})$ instead of the receiver equivalent resonant frequency $1/(2\pi\sqrt{L_R{}'C_R})$, calculated as 100.3 kHz. Furthermore, to "shift" the power curves, the transmitter capacitance is recompensated with $C_T{}' = 48$ nF, resulting in the performance shown in Fig. 17(b).

After extending the analysis and verification to a WPT system with relay coil-resonator, the theory can be generalized to analyzed WPT systems with multiple relay coil-resonators. Such theory and design guidelines are included in the Appendix.

V. Conclusion

This article explores the largely unchartered research area of WPT systems in which the presence of intended metallic object is inevitable. Such metallic objects increase the system matrix by one order. By reducing such matrices by one order mathematically to form a reduced-order model and comparing it with the original matrix without the metallic object, the effects of the metallic object can be theoretically quantified. The analysis indicates that the reduction of energy efficiency and power transfer capability caused by the metallic object of low resistance is due more to the redistribution of the magnetic field that decreases the mutual coupling between the transmitter and receiver coils than to the conduction loss in the metallic object. Such effects are reflected in the reduction of effective mutual coupling between the transmitter and receiver coils. Due to changes in the equivalent system parameters, the optimal operating frequency for maximizing energy efficiency and power transfer capability is also shifted by the metallic object.

The analysis leads to new engineering principles for enhancing the performance of a WPT system with intended metallic object of low resistance. The twofold principles involve the combined use of: 1) recompensating the resonant circuit to the shifted resonant frequency, and 2) redesigning the transmitter coil to maximize the equivalent mutual inductance between the transmitter and receiver coils. While the reduced-order model provides information for the new compensation capacitor for the resonant circuit, the equivalent mutual inductance between the transmitter coil and receiver coil (M'_{TR}) can be maximized by shortening the distance between the transmitter and receiver coils and simultaneously selecting a dimension ratio X (i.e., a ratio of the diameter of the transmitter and metallic object) away from unity in order to reduce the mutual coupling of the transmitter and the metallic object. The novel methodology has been successfully applied to WPT systems with and without relay resonators. The theory has been extended to WPT systems with N relay resonators and the extended theory is included in the Appendix.

APPENDIX

In this appendix, the analysis and recompensation methodology are generalized to *N*-coil systems. Reduced-order model is provided for both 1-ring and 2-ring systems in Section A and a compensation methodology is provided in Section B.

A. Reduced-Order Models

Fig. 3 shows an *N*-coil WPT system with two corona rings, whose self-inductances are denoted as L_{C1} and L_{C2}. $M_{\mathrm{k}C1}$ ($M_{\mathrm{k}C2}$) will later be used to denote the mutual inductance between the *k*th coil and L_{C1} (L_{C2}). One ring is placed between Tx (transmitter coil) and the first repeater; the other ring is between Rx (receiver coil, which is the *N*th coil in the string) and the last repeater (the (N−1)th coil). This is used to demonstrate the case with HV insulation strings on HV transmission towers. Note that in the following analyses, R_C is considered as zero for simplicity.

When there is only one ring in the system, in which we consider only the corona ring near Tx, the system characteristics can be described with the matrix expression in (26), shown at the bottom of this page. The reduced-order model matrix for this 1-ring, *N*-coil system is found to be (27), shown at the bottom of this page, in which

$$L_{kk}{}' = L_{kk} - \frac{{M_{kC1}}^2}{L_{C1}}, \text{ for diagonal elements} \tag{29}$$

$$M_{kj}{}' = M_{kj} - \frac{M_{kC1}M_{jC1}}{L_{C1}}, \text{ for any } k \neq j. \tag{30}$$

$$\begin{bmatrix} V_{\mathrm{IN}} \\ 0 \\ 0 \\ \vdots \\ 0 \\ 0 \end{bmatrix} = \begin{bmatrix} j(\omega L_1 - \frac{1}{\omega C_1}) & & & & & \\ +R_1 & j\omega M_{1C1} & j\omega M_{12} & \cdots & j\omega M_{1(N-1)} & j\omega M_{1N} \\ j\omega M_{1C1} & j\omega L_{C1} & j\omega M_{2C1} & \cdots & j\omega M_{(N-1)C1} & j\omega M_{NC1} \\ j\omega M_{12} & j\omega M_{2C1} & j(\omega L_2 - \frac{1}{\omega C_2}) & & & \\ & & +R_2 & \cdots & j\omega M_{2(N-1)} & j\omega M_{2N} \\ \vdots & \vdots & \vdots & \ddots & \vdots & \vdots \\ j\omega M_{1(N-1)} & j\omega M_{(N-1)C1} & j\omega M_{2(N-1)} & \cdots & j(\omega L_{N-1} - \frac{1}{\omega C_{N-1}}) & \\ & & & & +R_{N-1} & j\omega M_{(N-1)N} \\ j\omega M_{1N} & j\omega M_{NC1} & j\omega M_{2N} & \cdots & j\omega M_{(N-1)N} & j(\omega L_N - \frac{1}{\omega C_N}) \\ & & & & & +R_N + R_L \end{bmatrix} \cdot \begin{bmatrix} I_1 \\ I_C \\ I_2 \\ \vdots \\ I_{(N-1)} \\ I_N \end{bmatrix} \tag{26}$$

$$\begin{bmatrix} V_{\mathrm{IN}} \\ 0 \\ \vdots \\ 0 \\ 0 \end{bmatrix} = \begin{bmatrix} j(\omega L_1{}' - \frac{1}{\omega C_1}) + R_1 & j\omega M_{12}{}' & \cdots & j\omega M_{1(N-1)}{}' & j\omega M_{1N}{}' \\ j\omega M_{12}{}' & j(\omega L_2{}' - \frac{1}{\omega C_2}) + R_2 & \cdots & j\omega M_{2(N-1)}{}' & j\omega M_{2N}{}' \\ \vdots & \vdots & \ddots & \vdots & \vdots \\ j\omega M_{1(N-1)}{}' & j\omega M_{2(N-1)}{}' & \cdots & j(\omega L_{N-1}{}' - \frac{1}{\omega C_{N-1}}) + R_{N-1} & j\omega M_{(N-1)N}{}' \\ j\omega M_{1N}{}' & j\omega M_{2N}{}' & \cdots & j\omega M_{(N-1)N}{}' & j(\omega L_N{}' - \frac{1}{\omega C_N}) \\ & & & & +R_N + R_L \end{bmatrix} \cdot \begin{bmatrix} I_1 \\ I_2 \\ \vdots \\ I_{(N-1)} \\ I_N \end{bmatrix} \tag{27}$$

$$\begin{bmatrix} V_{\mathrm{IN}} \\ 0 \\ 0 \\ \vdots \\ 0 \\ 0 \\ 0 \end{bmatrix} = \begin{bmatrix} j(\omega L_1 - \frac{1}{\omega C_1}) & & & & & & \\ +R_1 & j\omega M_{1C1} & j\omega M_{12} & \cdots & j\omega M_{1(N-1)} & j\omega M_{1C2} & j\omega M_{1N} \\ j\omega M_{1C1} & j\omega L_{C1} & j\omega M_{2C1} & \cdots & j\omega M_{(N-1)C1} & j\omega M_{C1C2} & j\omega M_{NC1} \\ j\omega M_{12} & j\omega M_{2C1} & j(\omega L_2 - \frac{1}{\omega C_2}) + R_2 & \cdots & j\omega M_{2(N-1)} & j\omega M_{2C2} & j\omega M_{2N} \\ \vdots & \vdots & \vdots & \ddots & \vdots & \vdots & \vdots \\ j\omega M_{1(N-1)} & j\omega M_{(N-1)C1} & j\omega M_{2(N-1)} & \cdots & j(\omega L_{N-1} - \frac{1}{\omega C_{N-1}}) & & \\ & & & & +R_{N-1} & j\omega M_{(N-1)C2} & j\omega M_{(N-1)N} \\ j\omega M_{1C2} & j\omega M_{C1C2} & j\omega M_{2C2} & \cdots & j\omega M_{(N-1)C2} & j\omega L_{C2} & j\omega M_{NC2} \\ j\omega M_{1N} & j\omega M_{NC1} & j\omega M_{2N} & \cdots & j\omega M_{(N-1)N} & j\omega M_{NC2} & j(\omega L_N - \frac{1}{\omega C_N}) \\ & & & & & & +R_N + R_L \end{bmatrix} \cdot \begin{bmatrix} I_1 \\ I_{C1} \\ I_2 \\ \vdots \\ I_{(N-1)} \\ I_{C2} \\ I_N \end{bmatrix} \tag{28}$$

Similarly, a 2-ring, *N*-coil system can be described using the matrix expression in (28), shown at the bottom of previous page. To obtain its reduced-order model, L_{C2} and all its related mutual inductance $M_{\mathrm{k}C2}$ need to be rewritten as

$$L_{C2}{}' = L_{C2} - \frac{{M_{C1C2}}^2}{L_{C1}} \tag{31}$$

$$M_{kC2}{}' = M_{kC2} - \frac{M_{kC1}M_{kC2}}{L_{C1}}. \tag{32}$$

The equivalent model of the whole system is then obtained also as in (27), but with equivalent self- and mutual inductance parameters derived as

$$L_{kk}{}' = L_{kk} - \frac{{M_{kC1}}^2}{L_{C1}} - \frac{{M_{kC2}}'^2}{L_{C2}{}'}, \text{for diagonal elements} \tag{33}$$

$$M_{kj}{}' = M_{kj} - \frac{M_{kC1}M_{jC1}}{L_{C1}} - \frac{M_{kC2}{}'M_{jC2}{}'}{L_{C2}{}'}, \text{for any } k \neq j. \tag{34}$$

Simulations have been carried out to prove the above reduced-order models to be correct. Notice how the equations follow the same patterns as in the two-coil system, enabling this model to be further extended to multiple ring systems.

B. Recompensation

In practical domino systems utilized in HV insulators, inductors and capacitors are embedded in insulation discs and then assembled into a string. Corona rings are then added to the sides of the string. The whole system is fixed at this stage and the only remaining variables for adjustment are the Tx and Rx compensation capacitors and load resistor. Therefore, we can assume all coil inductance, repeater compensation capacitance, and distances between any two coils to be fixed. There are some important factors that have been observed and will become the basis of transmitter and receiver capacitor compensation later.

1) Efficiency is dependent on compensation capacitor C_N for the receiver Rx (last coil in system), but independent of C_1 for the transmitter Tx (first coil). For any C_N, efficiency varies with different operating frequencies and load resistances R_L. Efficiency of the system can be expressed as

$$\eta = \{C_N, R_L, f\}. \tag{35}$$

Every C_N corresponds to an optimal efficiency η_{opt} at different frequencies f_{opt} and loads R_{Lopt}. The value of η_{opt} is different for different C_N

$$\eta_{\mathrm{opt}} = \{C_N, R_{\mathrm{Lopt}}, f_{\mathrm{opt}}\}. \tag{36}$$

Output power is dependent on both C_N and C_1. Similar to efficiency, it can be expressed as

$$P_O = \{C_1, C_N, R_L, f\}. \tag{37}$$

For a fixed set of C_N, R_L, and f, there exists a value of C_1 that results in the maximum output power $\mathrm{P_{Omax}}$.

These principles apply for any domino system with or without corona ring. Due to the independency of efficiency on C_1, it is better to compensate C_N before C_1 for domino systems. A diagram of suggested compensation procedures for domino WPT system with fixed resonator parameters is shown in Fig. 18.

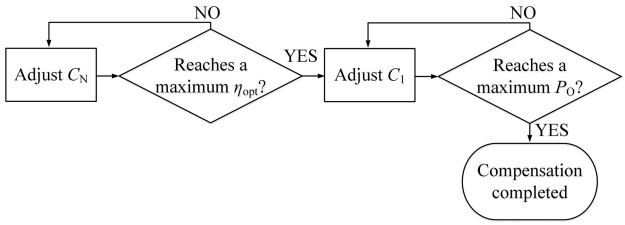

Fig. 18. Suggested compensation procedure for domino WPT systems.

REFERENCES

[1] G. A. Covic and J. T. Boys, "Inductive power transfer," *Proc. IEEE*, vol. 101, no. 6, pp. 1276–1289, Jun. 2013.
[2] S. Y. R. Hui, "Planar wireless charging technology for portable electronic products and Qi," *Proc. IEEE*, vol. 101, no. 6, pp. 1290–1301, Jun. 2013.
[3] J. Ho, S. Kim, and A. Poon, "Midfield wireless powering for implantable systems [Invited paper]," *Proc. IEEE*, vol. 101, no. 6, pp. 1369–1378, Jun. 2013.
[4] A. Ahmad, M. Alam, and R. Chabaan, "A comprehensive review of wireless charging technologies for electric vehicles," *IEEE Trans. Transp. Electrific.*, vol. 4, no. 1, pp. 38–63, Mar. 2018.
[5] F. Kempe, M. Herbrich, and D. Münch, "Sensor arrangement and rolling bearing having such a sensor arrangement," Patent Appl. WO2016/000694A1, Jun. 30, 2014.
[6] C. Zhang, D. Y. Lin, and S. Y. R. Hui, "Ball-joint wireless power transfer system," *IEEE Trans. Power Electron.*, vol. 33, no. 1, pp. 565–572, Jan. 2018.
[7] X. Liu, H. Swaans, W. Chan, K. Low, and K. Chan, "Methods and systems for detecting foreign objects in a wireless charging system," U.S. Patent 9 178 361 B2, Nov. 3, 2015.
[8] J. Patino, S. Thekkevalappil, and S. Sibecas, "Energy transfer optimization by detecting and mitigating magnetic saturation in wireless charging with foreign object detection," U.S. Patent 9 391 470 B2, Jul. 12, 2016.
[9] H. Dorairaj, R. Kumar, and S. Ganguly, "Foreign object detection in inductive coupled devices," U.S. Patent 8 575 944 B2, Nov. 5, 2013.
[10] L. Xiang, Z. Zhu, J. Tian, and Y. Tian, "Foreign object detection in a wireless power transfer system using symmetrical coil sets," *IEEE Access*, vol. 7, pp. 44622–44631, 2019.
[11] F. Borngraber, "Foreign object detection," PCT Patent Appl. WO 2014/064489, May 1, 2014.
[12] W. X. Zhong, C. K. Lee, and S. Y. R. Hui, "General analysis on the use of Tesla's resonators in domino forms for wireless power transfer," *IEEE Trans. Ind. Electron.*, vol. 60, no. 1, pp. 261–270, Jan. 2013.
[13] C. Zhang, D. Lin, N. Tang, and S. Y. R. Hui, "A novel electric insulation string structure with high-voltage insulation and wireless power transfer capabilities," *IEEE Trans. Power Electron.*, vol. 33, no. 1, pp. 87–96, Jan. 2018.
[14] W. X. Zhong and S. Y. R. Hui, "Maximum energy efficiency tracking for wireless power transfer systems," *IEEE Trans. Power Electron.*, vol. 30, no. 7, pp. 4025–4034, Jul. 2015.

Hui Wen Rebecca Liang (Student Member, IEEE) received the B.S. and M.S. degrees in electrical and electronic engineering from National Cheng Kung University, Tainan, Taiwan, in 2013 and 2015, respectively. She is currently working toward the Ph.D. degree with the University of Hong Kong, Hong Kong.

From 2015 to 2017, she was an Analog Circuit Engineer with Chroma ATE (Advanced Technology Research Center), Taiwan. Her research interests include power electronics, wireless power transfer, dc–dc power converters, and renewable energy conversion.

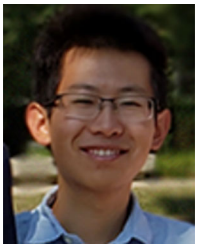

Hanwei Wang received the B.S. degree from the Department of Physics, Tsinghua University, Beijing, China, in 2019. He is currently working toward the Ph.D. degree with the Department of Electrical and Computer Engineering, University of Illinois at Urbana-Champaign (UIUC), Urbana, IL, USA.

His research interests include metamaterials, optical force microscopy, magnetic resonance imaging, and wireless power transfer, apart from developing artificial electromagnetic materials' applications in biomedical imaging and biosensors.

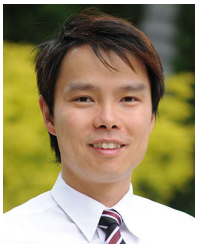

Chi-Kwan Lee (Senior Member, IEEE) received the B.Eng. and Ph.D. degrees in electronic engineering from the City University of Hong Kong, Hong Kong, in 1999 and 2004, respectively.

He is currently an Associate Professor with the Department of Electrical and Electronic Engineering, The University of Hong Kong. From 2008 to 2011, he was a Lecturer of Electrical Engineering with the Hong Kong Polytechnic University, Hong Kong. Since 2010, he has been a Visiting Researcher with Imperial College London, London, U.K. In 2006, he joined as a Research Fellow with the Centre of Power Electronics, City University of Hong Kong. From 2004 to 2005, he was a Postdoctoral Research Fellow with the Power and Energy Research Centre, National University of Ireland, Galway, Ireland. He is a co-inventor of the electric springs and planar EMI filter. His current research interests include wireless power transfer, clean energy technologies, and smart grids.

Dr. Lee was the recipient of the IEEE POWER ELECTRONICS TRANSACTIONS First Prize Paper Award for his work on "Mid-Range Wireless Power Transfer" in 2015.

S. Y. Ron Hui (Fellow, IEEE) received the B.Sc. (hons.) degree in electrical and electronic engineering from the University of Birmingham, Birmingham, U.K., in 1984, and the D.I.C. and Ph.D. degrees in electrical engineering from the Imperial College London, London, U.K., in 1987.

He is presently the Philip Wong Wilson Wong Chair Professor with The University of Hong Kong and a Chair Professor with the Imperial College London. He is the author or co-author of more than 260 refereed journal publications and more than 60 of his patents have been adopted by the industry. His inventions on wireless charging platform technology underpin key dimensions of Qi, the world's first wireless power standard, with freedom of positioning and localized charging features for wireless charging of consumer electronics. He also developed the photoelectrothermal theory for LED systems. His research interests include power electronics, wireless power, sustainable lighting, and smart grid.

Prof. Hui was the recipient of the IEEE Rudolf Chope R&D Award and the IET Achievement Medal (The Crompton Medal) in 2010 and the IEEE William E. Newell Power Electronics Award in 2015. He is a fellow of the Australian Academy of Technological Sciences and Engineering since 2010, the U.S. Academy of Inventors since 2018, and the Royal Academy of Engineering, U.K. since 2016.